Journal of Inflammation Research

Dovepress
Taylor & Francis Group

Open Access Full Text Article

ORIGINAL RESEARCH

Multi-Omics Analysis Combined with Machine Learning Identified FABP4 in Smooth Muscle Cells as a Pathogenic Factor in Atherosclerosis

Yinyu Wang[1], Tingting Shang[1], Rui Cai[2], Cuiping Wang[1]

[1]Department of Cardiology, Affiliated Hospital of Jiangsu University, Zhenjiang, People's Republic of China; [2]Department of Cardiology, The Affiliated Yancheng Maternity & Child Health Hospital of Yangzhou University, Yancheng, People's Republic of China

Correspondence: Cuiping Wang, Department of Cardiology, Affiliated Hospital of Jiangsu University, No. 438 Jiefang Road, Jingkou District, Zhenjiang City, Jiangsu Province, People's Republic of China, Email wangcuipingpeople@hotmail.com

Background: Atherosclerosis is the pathological basis of coronary heart disease, stroke, and peripheral arterial disease. Smooth muscle cells (SMCs) play a crucial role in atherosclerotic pathogenesis. However, effective drugs and therapy targeting SMCs for treating atherosclerosis are still lacking.

Methods: We utilized single-cell RNA sequencing (scRNA-seq) (GSE155512 and GSE159677) and array data (GSE43292 and GSE125771) to identify Scissor+ SMCs (SMCs positively associated with atherosclerosis) and Scissor- SMCs (SMCs negatively associated with atherosclerosis) by using Scissor package. We analyzed their functional changes, cell-cell communication, and differentiation potential. Machine learning techniques were employed to analyze the marker in SMCs of atherosclerosis. qRT-PCR was used to examine the expression of these genes in MOVAS stimulated by ox-LDL. Potential inhibitors of the identified proteins were predicted, and their binding sites were analyzed.

Results: We identified 475 Scissor+ SMCs and 1363 Scissor- SMCs. Functional enrichment analysis revealed that Scissor+ SMCs exhibited downregulation of Rho-related pathways, while pro-inflammatory pathways were upregulated. Cell-cell communication analysis indicated tighter interactions between SMCs and endothelial cells. Differential expression analysis identified 20 genes highly expressed in both scRNA-seq and array data. The LASSO regression, random forest, support vector machine and receiver operating characteristic curve suggested a strong correlation between fatty acid-binding protein 4 (FABP4) and atherosclerosis. The qRT-PCR results showed that FABP4 was highly expressed in MOVAS stimulated by ox-LDL. Drug prediction revealed that (S)-RP-6306 acted as an inhibitor, via forming a polar bond with Arg-126. In vitro experiments confirmed that (S)-RP-6306 significantly reduced the expression of FABP4.

Conclusion: Scissor+ SMCs differed significantly from Scissor- SMCs in cellular function, cell-cell communication, and differentiation potential. The high expression of FABP4 in this subgroup of SMCs presented a promising therapeutic target for atherosclerosis, with (S)-RP-6306 showing potential as a drug targeting FABP4.

Keywords: atherosclerosis, smooth muscle cell, machine learning, molecular docking

Introduction

Atherosclerosis is a chronic and progressive cardiovascular disease primarily characterized by the accumulation of lipids in the arterial walls. Historically, atherosclerosis was considered largely a disorder of lipid storage, but contemporary research has revealed that inflammation plays a crucial role throughout the entire progression of the disease.[1] This disease is complex and multifaceted, involving not only lipid deposition but also a series of interconnected pathological processes including inflammation, endothelial injury, plaque rupture and thrombus formation.[2] Inflammation is a central feature of atherosclerosis, and various types of inflammatory cells contribute significantly to its development and progression. These include macrophages, which are known for their role in engulfing and processing lipids, neutrophils, which exacerbate inflammation through the release of neutrophil extracellular traps, and lymphocytes such

Received: 18 February 2025
Accepted: 19 July 2025
Published: 26 July 2025

Graphical Abstract

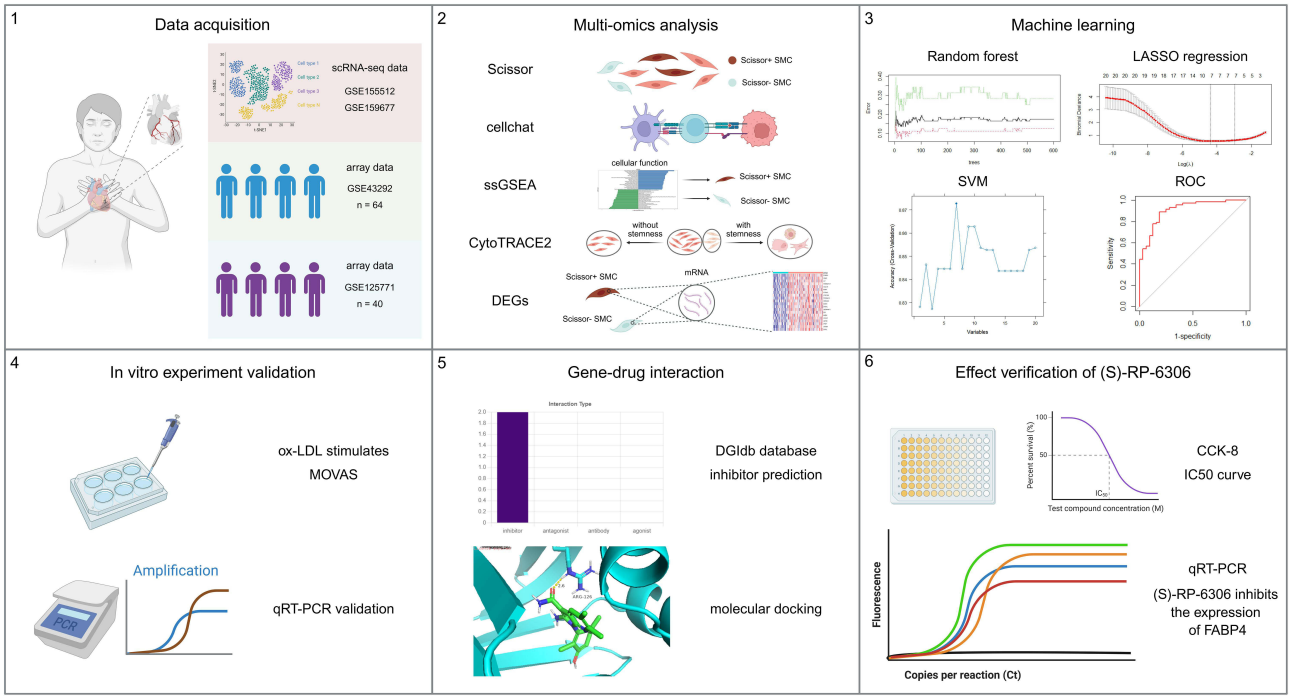

as T and B cells, which are involved in the adaptive immune response.[3–6] In addition to the aforementioned immune cells, other non-inflammatory cells also play crucial roles in atherogenesis.

Smooth muscle cells (SMCs), in particular, contribute to the formation of atherosclerotic plaques, impacting not only their composition but also their stability. Research has demonstrated that a substantial proportion, approximately 30% to 70%, of the foam cells found within these plaques are derived from SMCs that have undergone a process known as transdifferentiation.[7] This process involves the transformation of SMCs into foam cells, which are lipid-laden and contribute to plaque formation. These cells also release extracellular traps to promote the progression of atherosclerosis through the activation of the TLR4-MYD88 signaling pathway, which is involved in the immune response and inflammation.[8] Additionally, SMCs can also transdifferentiate into other cell types such as myofibroblast-like cells and osteochondral-like cells, further contributing to vascular sclerosis. This transdifferentiation process has significant implications for the stability of atherosclerotic plaques, as it leads to changes in the extracellular matrix and contributes to the overall rigidity of the arterial walls.[9] During the above process, SMCs also undergo a phenotypic transition from a "contractile" to a "synthetic" state. In the contractile phenotype, SMCs are primarily involved in maintaining vascular tone and structure, while in the synthetic phenotype, they proliferate, migrate, and lose their original contractile function. This transition is a key factor in the development and progression of atherosclerosis, as it contributes to plaque formation and vascular remodeling.[10] Although there has been significant progress in developing nanomedicine (NM) targeting Glucagon-like peptide-1 receptor (GLP-1R) and sirtuin 1 (SIRT1) on SMCs, such as GLP-1R agonist liraglutide and ICG/SRT@HSA-pept NMs,[11,12] the atherogenic effects of SMCs are complex and not yet fully understood. Current research is ongoing to develop more effective strategies for preventing atherosclerosis by targeting SMCs and understanding their multifaceted roles in the disease.

Single-cell RNA sequencing (scRNA-seq) technology has emerged as a powerful tool for studying the cellular heterogeneity of disease. This technology allows researchers to identify new cell subgroups, understand their specific roles in disease mechanisms, uncover detailed insights into the pathology of diseases and facilitate drug

development.[13,14] Despite its advantages, scRNA-seq technology has some limitations, including high costs and insufficient sample size. Although the current cost has been greatly decreased, the issue of sample size has not been well resolved.[15] To address this limitation, integrating scRNA-seq data with bulk RNA sequencing (RNA-seq) data can provide a more comprehensive and accurate understanding of the disease.

In this study, scRNA-seq and array data were utilized to analyze the pathogenic subgroups of SMCs in atherosclerosis. Due to the lack of suitable RNA seq data, array data served as an alternative. By identifying signature proteins associated with these cells, the research aims to offer new insights into clinical prevention, therapy, and drug design, ultimately contributing to the development of more effective strategies for the diagnosis and treatment of atherosclerosis.

Materials and Methods

Acquisition and Preprocessing of Single-Cell RNA Sequencing Data

The scRNA-seq data of human carotid atherosclerotic plaques were obtained from the Gene Expression Omnibus (GEO) database (https://www.ncbi.nlm.nih.gov/geo/), which collects, stores, and shares a large amount of genomic data from global research institutions. According to item 1 and 2 of Article 32 of the Measures for Ethical Review of Life Science and Medical Research Involving Human Subjects dated February 18, 2023, China, this study does not require approval from the ethics committee. Datasets GSE155512 and GSE159677 were selected for analysis by using the keyword "atherosclerosis" for retrieval. The "Read10×" function in the Seurat package (version 5.0.2) in R project (version 4.3.0) was employed to convert the data into dgCMatrix.[16] The cells included in the analysis met the following criteria: Firstly, they had an nFeature RNA ranging from 200 to 8000. Secondly, the proportion of mitochondrial genes was less than 10%. After filtering, "LogNormalize" function in Seurat package was used to normalize the data, and harmony package can mitigate batch effects between different samples to enhance data comparability. Subsequently, "RunUMAP" function in Seurat package can perform uniform manifold approximation and projection (UMAP) to simplify the data, which is one of the commonly used non-linear dimensionality reduction. Clustering analysis was performed by "FindNeighbors" and "FindClusters" functions. The resolution was set to 0.5 in the "FindClusters" function. All cells were annotated according to the cell markers from CellMarker 2.0 database (http://bio-bigdata.hrbmu.edu.cn/CellMarker/index.html) and existing research.

Acquisition and Preprocessing of Array Data

The array data of human carotid atherosclerotic plaques were also retrieved from the GEO database. Owing to the small sample size of most individual datasets, multiple datasets are merged for analysis. GSE43292 (32 normal samples and 32 diseased samples) and GSE125771 (40 diseased samples) were chosen for Subsequent analysis, with the reason that both datasets were measured using affymatrix array, satisfying the needs of array merging. The.CEL files were processed using the affy and oligo packages. Data normalization was used quantile method via "voon" function in limma package to enhance comparability.[17] Batch effects were corrected by using the "combat" function in sva package, ensuring the merged data approached a normal distribution.[18]

Definition of Atherosclerosis Phenotype-Associated Cells

The Scissor package was used to identify phenotype-associated cells by integrating bulk and scRNA-seq data.[19] Considering the phenotype-associated information contained in the data, we opted for the "binomial" parameter instead of "cox" or "gaussian" to define the cell associated with atherosclerotic phenotype. In this process, the default of the parameter "cutoff" is usually 20%, which indicates the sum of Scissor- (negatively associated with the phenotype) and Scissor+ (positively associated with the phenotype) cells do not exceed 20% of all cells. The reliability of results can be estimated via "reliability.test" function in the Scissor package, with the nfold set to 10. If the p value of this reliability test is less than 0.05, the definition of phenotype-associated cells can be considered reliable.

Cell-Cell Communication Analysis

The CellChat package (version 2.1.2) was employed for cell-cell communication analysis based on ligand-receptor interactions.[20] The "createCellChat" function created a CellChat object from a Large Seurat object, utilizing CellChatDB. human as the reference database. Preprocessing of the CellChat object was conducted via the "subsetData" function. Subsequent steps included identifying over-expressed genes by using the "identifyOverExpressedGenes" function and detecting over-expressed ligand-receptor pairs with the "identifyOverExpressedInteractions" function. The "projectData" function projected the ligand-receptor pairs onto the PPI network. Cell interaction probabilities were calculated using the "computeCommunProb" function, and the cell subtype with fewer than 10 cells were removed using the "filterCommunication" function. Communication outcomes across signaling pathways were computed using the "computeCommunProbPathway" function, followed by integration of cell communication results between cell types via the "aggregateNet" function. Visual representation of the results was achieved using the "netVisual_circle" and "netVisual_bubble" functions. The cell-cell communication analysis was performed on both Scissors+ and Scissors- cells in accordance with the above methodology.

Functional Enrichment Analysis

Single-sample gene set enrichment analysis (ssGSEA) is a method used for single sample gene set enrichment analysis. It evaluates the enrichment level of gene sets by comparing the expression patterns of genes in a single sample with the expression patterns of predefined gene sets.[21] The msigdbr package was used to extract gene sets for various signaling pathways, focusing on Kyoto Encyclopedia of Genes and Genomes (KEGG) (https://www.kegg.jp/) and Reactome (https://reactome.org/) database. Gene expression matrix of SMC was extracted from the Large Seurat object. The analysis was performed by GSEABase and GSVA packages. Enrichment scores for pathways in Scissor+ SMCs and Scissor- SMCs were compared using the limma package to identify pathways significantly differentially expressed in Scissor+ SMCs.

Cellular Potency Prediction

CytoTRACE 2 is a computational method that utilizes scRNA-seq data to predict cellular potency category and potency score.[22] Potency score ranges continuously from 0 (differentiated) to 1 (totipotent), with potency categories classified as "Differentiated", "Unipotent", "Oligopotent", "Multipotent", "Pluripotent" and "Totipotent". To analyze the difference of cellular potency category between Scissor+ SMCs and Scissor- SMCs, the Seurat-formatted file was extracted and analyzed using the "cytotrace2" function within the CytoTRACE 2 package. During this process, the count from the Seurat-formatted file of SMCs was utilized, specifying the species as "human". Visualization was performed with the "plotData" function. The differentiation categories of Scissor-, Scissor0, and Scissor+ SMCs were quantified separately. Statistical differences in the potency score between Scissor+ and Scissor- SMCs were assessed using the Wilcox method from the ggpubr package, and visualizations were generated accordingly.

Differentially Expressed Genes

For scRNA-seq data, "FindMarkers" function was used to find differentially expressed genes (DEGs) between Scissor+ subgroup and Scissor- subgroup in SMCs, in which parameter were set to "logfc.threshold = 0.25" and "test.use = wilcox". For array data, the limma package is preferred over other packages. It employs functions such as "makeContrasts", "lmFit", "contrasts.fit", and "eBay" to conduct analysis on array data comparing the diseased group to the control group.

GO Enrichment Analysis

The clusterProfiler package was utilized to conduct Gene Ontology (GO) enrichment analysis on all upregulated DEGs, with a screening threshold of "P value < 0.05". GO enrichment analysis is primarily employed to identify whether genes within a specific gene set or functional module are enriched in particular biological processes. The results of this analysis can be categorized into three aspects: biological processes, cellular components, and molecular functions.

Machine Learning

Four machine learning approaches were utilized in this research. Random forest (RF) analysis was conducted using the randomForest package.[23] During this process, we evaluated 0–1000 decision trees and selected the tree with the lowest error rate as the optimal parameter (ntree). Subsequently, the rfcv function in the randomForest package was used to perform leave-one-out cross validation to validate the reliability of the results. Following this, the most relevant DEGs for atherosclerosis were determined based on the size of "MeanDecreaseGini". The least absolute shrinkage and selection operator (LASSO) regression was implemented via glmnet package.[24] Cross-validation was employed to identify the smallest lambda, and L-1 norm was applied in the LASSO regression to identify the DEGs associated with atherosclerosis. The support vector machine (SVM) is a powerful classification tool that has been used for filtering disease biomarkers, and this analysis was performed by e1071 package and caret package.[25] The results from the three methods were integrated, and a diagnostic model was constructed using the receiver operating characteristic (ROC) curve with the pROC package to compute the area under the curve (AUC).[26] A higher AUC value indicates a better model, and the DEG with the AUC closest to 1 was selected as the target for subsequent analysis of atherosclerosis.

Quantitative Reverse Transcriptase Polymerase Chain Reaction (qRT-PCR)

Murine aortic vascular smooth muscle cells (MOVAS) (ATCC, No. CRL-2797^{TM}) were treated with a 25 μg/mL concentration of oxidized low-density lipoprotein (ox-LDL) (Yiyuan Biotechnologies, Guangzhou, China, No. YB-002-1) and 0.2 μM (S)-RP-6306 (MedChemExpress, China, No. HY-145817A) for a duration of 4 days. RNA was subsequently extracted from these cells using the RNA-easy isolation reagent, followed by quantification of the RNA concentration using a spectrophotometer. Reverse transcription was performed based on the determined RNA concentration above. The reaction was conducted using SYBR Green as the fluorescent dye (Vazyme, Nanjing, China, No. R701-01, No. R123-01, No. Q312-02). The qRT-PCR program was set as follows: preincubation at 95°C for 30 seconds, amplification at 95°C for 10 seconds and 60°C for 30 seconds, followed by 60 cycles. If no amplification curve was observed, the number of cycles could be increased. The primer sequences used are listed in Table 1 (Sangon Biotech, Shanghai, China).

Western Blot

MOVAS were lysed in RIPA lysis buffer (Beyotime Biotechnology, China, No. P0013B) supplemented with a protease inhibitor cocktail. Before electrophoresis, Loading Buffer was added to the cell lysates. Subsequently, the proteins were separated by SDS-Polyacrylamide Gel Electrophoresis (SDS-PAGE) and then transferred onto a Polyvinylidene Difluoride (PVDF) membrane (Millipore, America, No. ISEQ00010). The membrane was blocked with 5% non-fat milk. The membrane was then incubated overnight at 4°C with primary antibodies, specifically anti-ACTA2 (diluted at 1:2000) (Abways Technology, Shanghai, China, No. CY1132) and anti-GAPDH (diluted at 1:50,000) (Proteintech, Wuhan, China, No. 60004-1-Ig). After that, the membrane was washed with TBST buffer and then incubated with a secondary antibody (diluted at 1:5000) for 1 hour at room temperature (Abways Technology, Shanghai, China, No. AB0101, No. AB0102). Following another round of washing with TBST buffer, the membrane was visualized using an ECL chemiluminescence kit (Abbkine Scientific Co., Ltd, Wuhan, China, No. BMU102). The grayscale values of the protein bands were measured using ImageJ software, with GAPDH serving as an internal reference control. The protein

Table 1 The Sequence of Primers

Gene	Forward	Reverse
FABP4	5'-CAAGGAAAGTGGCAGGCATGG-3'	5'-ACGCCCAGTTTGAAGGAAATCTC-3'
TNFRSF17	5'-CCGTGTCACTTGCGATGTTCC-3'	5'-AGAAGATCCAGAGCACCGTGTAC-3'
IFITM1	5'-ACAGGAAGATGGTGGGTGATACG-3'	5'-CAGACAACGATGACGACGATGG-3'
MZB1	5'-CTCTGCCACTGTTGCTACTGTTC-3'	5'-GAGCCGAGTACTTCTCTTCATCATC-3'
GAPDH	5'-CCTCGTCCCGTAGACAAAATG-3'	5'-TGAGGTCAATGAAGGGGTCGT-3'

expression level was calculated as the ratio of the grayscale value of the target band to that of the internal reference band. Each experiment was independently replicated in triplicate to ensure the reliability and reproducibility of the results.

CCK8 Assay

MOVAS cells were seeded in 96-well plates at a density of 5000 cells in 100 μL per well. After 24 hours of cultivation, the medium was replaced with fresh medium, and different concentrations of (S)-RP-6306 were added to the cell culture medium of each treatment group. Following a 24-hour incubation of the cells at 37°C, 10 μL of CCK8 (NCM Biotech, Suzhou, China, No. C6005) was added to each treatment group, and the cultures were further incubated for 1 hour. The absorbance (OD value) was measured at a wavelength of 450 nm using a microplate reader. Finally, GraphPad Prism 9 was employed to perform nonlinear regression and plot the curve. Each experiment was replicated in triplicate to ensure the reliability and reproducibility of the results.

Drug Prediction and Molecular Docking

The Drug Gene Interaction Database (DGIdb) (https://dgidb.org/) is a database that aggregates information on interactions between drugs and genes.[27] In this research, the database was utilized to retrieve compounds binding to targets, and molecular docking was performed on compounds that have not been confirmed to bind yet. Compound structures were obtained from the PubChem database (https://pubchem.ncbi.nlm.nih.gov/), and protein structures from the PDB database (https://www.rcsb.org/).[28,29] The structures were preprocessed by ChemBio3D (version 14.0) and AutoDockTools (1.5.6). Finally, Vina (version 1.1.2) was used for docking analysis, and potential binding sites were visualized and analyzed by PyMOL (version 2.4.1).

Results

Preprocessing of Sequencing Data and Identification of Atherosclerosis-Associated Cells

After filtering scRNA-seq data, 44281 cells were included in the research and they were divided into 25 cell clusters according to the cluster analysis (Figure 1A and Figure S1A–E). On the other hand, the vast majority of array data satisfy normality via Q-Q test after normalization and removal of batch effects (Figure S1F–H). In the scRNA-seq data, the clusters were annotated according to the cell markers (Figure 1B and Table 2). The clusters were annotated as follows: SMCs (cluster 5, 8, 11, 14), endothelial cells (ECs) (cluster 7, 10, 21), monocyte/macrophages (cluster 3, 6, 12, 15, 16), T / NK cells (cluster 0, 1, 2), B cells (cluster 13, 18, 24), dendritic cells (DCs) (cluster 9, 22), fibroblasts (cluster 4), MAST cells (cluster 17), pericytes (cluster 19) and progenitor cells (cluster 20, 23) (Figure 1C). Moreover, clusters 0, 1 and 2 were extracted and subjected to further re-clustering analysis to obtain accurate cell annotation results with the reason that T cells and NK cells mixed together in these clusters (Figure S2). Ultimately, the 44281 cells were categorized into 13 distinct types (Figure 1D and E). Through analysis with Scissor package, we identified 4497 Scissor- cells and 2535 Scissor+ cells (Figure 1F and G). In this process, alpha was set to 0.05, and the sum of Scissor- cells and Scissor+ cells accounted for 15.88%, which was below the 20% cutoff. The reliability test show that test statistic was 0.925, and the p value was less than 0.001. This result is a testament to the reliability and the potential impact of the insights gleaned from this in-depth examination of the cellular landscape.

Cell-Cell Communication Analysis

To investigate how SMCs interact with other cells to promote atherosclerosis, we compared the cell-cell communication patterns between Scissor+ and Scissor- subgroups of SMCs. The cell-cell communication analysis revealed that, compared to Scissor- subgroup, although there was no significant difference in the number of interactions between Scissor+ SMCs with Scissor+ ECs whether SMCs acted as sources or targets, the interaction weight between the two cells was significantly enhanced. Moreover, the number and weight of interaction between SMCs with naive T cells were notably reduced in Scissor+ subgroup (Figure 2A–D). Among all analyzed pathways, when Scissor+ SMCs acted as sources, the CD23 (SMCs-ECs) and THBS (SMC-ECs) pathways were significantly upregulated, whereas the IL4 (SMC-

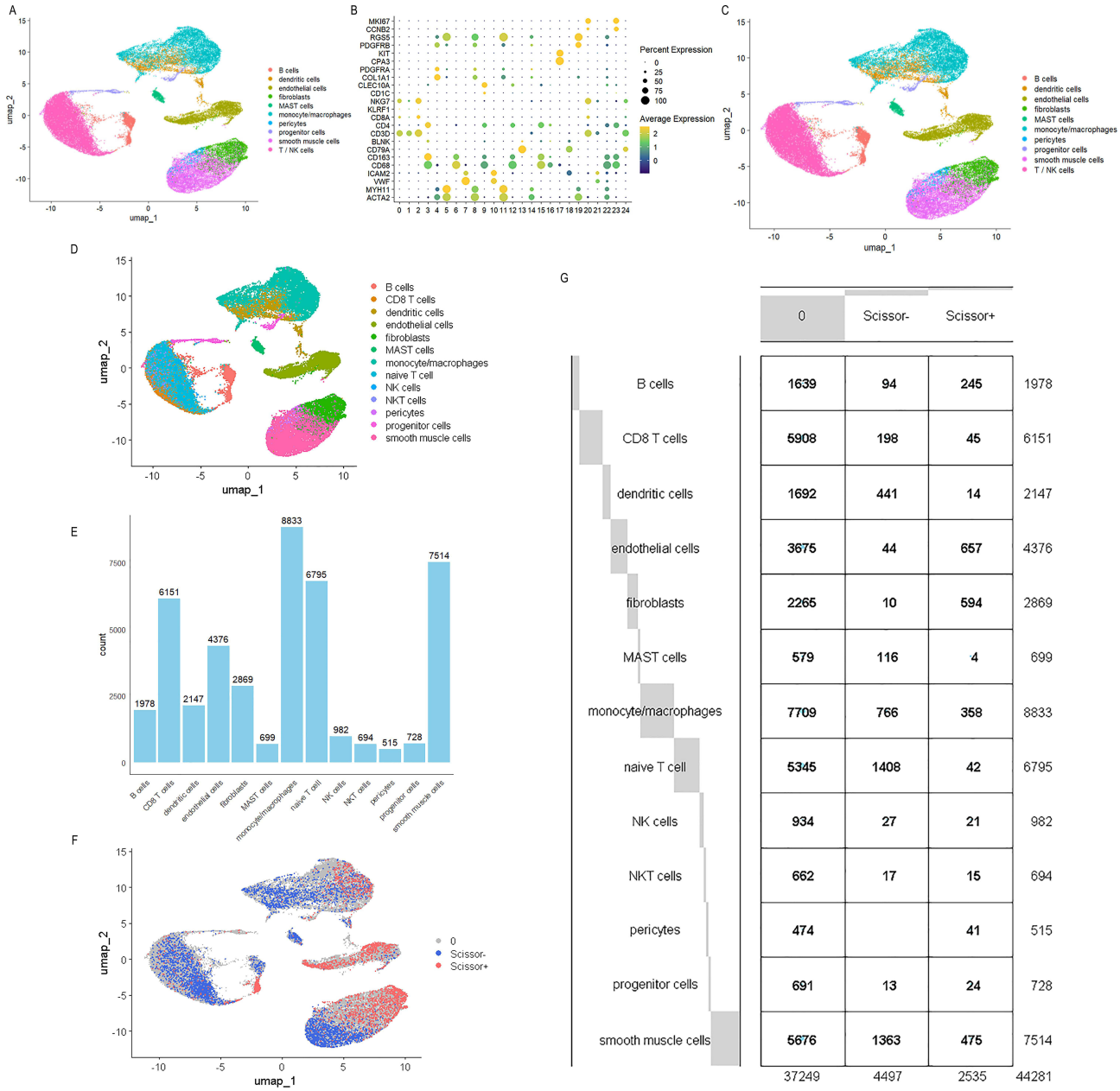

Figure 1 Identification of Scissor+ SMCs and Scissor- SMCs. (**A**) UMAP plot of 44281 cells which were separated into 25 clusters. (**B**) The expression of cell markers in 25 clusters. (**C**) The UMAP plot of cells after annotation. (**D**) The UMAP plot of cell annotation after T / NK cells being re-clustered and re-annotated. (**E**) The histogram of counts for various cell types. (**F**) The UMAP plot of Scissor+ cells and Scissor- cells. (**G**) The balloonplot showing the proportion of each cell type in Scissor+, Scissor-, and Scissor0 subgroups.

DCs) pathway was significantly downregulated. Conversely, when Scissor+ SMCs acted as targets, the Complement (ECs-SMCs) and PARs (ECs-SMCs) pathways were significantly upregulated, while the ADGRE (naive T cell-SMCs) and Glutamate (monocyte/macrophages-SMCs) pathways were significantly downregulated (Figure 2E–H). Particularly, the IL-4, complement, and PARs pathways have been demonstrated to influence the involvement of SMCs in the process of atherosclerosis, whereas the specific contributions of other pathways such as ADGRE, Glutamate, CD23, and THBS remain unclear. It is noteworthy that the most significantly downregulated pathways (L4, ADGRE, and Glutamate) are all anti-inflammatory pathways, whereas the upregulated pathways (CD23, THBS, Complement, and PARs) are pro-inflammatory pathways.

https://doi.org/10.2147/JIR.S519114

Table 2 The Markers of Cell Types

Cell Type	Markers	Reference
Smooth muscle cell	ACTA2, MYH11	[30]
Endothelial cell	VWF, ICAM2	[31,32]
Monocyte/ macrophage	CD68, CD163	[33]
B cell	CD79A, BLNK	[34]
$CD4^+$ T cell	CD3D, CD4	[35]
$CD8^+$ T cell	CD3D, CD8A	[35]
Naive T cell	CD4, CD8A	[35]
NKT cell	CD3D, KLRF1	[35]
NK cell	NKG7, KLRF1	[32,36]
Dendritic cell	CD1C, CLEC10A	[37]
Fibroblast	COL1A1, PDGFRA	[38,39]
MAST cell	CPA3, KIT	[32,40]
Pericyte	PDGFRB, RGS5	[41,42]
Progenitor cell	CCNB2, MKI67	[43]

Functional Enrichment Analysis

To explore the differences of cellular functional between Scissor+ SMCs and Scissor- SMCs. We analyzed all pathways in KEGG database and REACTOME database. In Scissor+ SMCs, some pathways were significantly downregulated, such as Rho GTPases activate rocks, Rho GTPases activate CIT, and Rho GTPases activate PAKs. Conversely, complement and coagulation cascades, interferon alpha beta signaling, and cell adhesion molecules CaMs were significantly upregulated (Figure 3A–C). Additionally, we divided the signaling pathway into three parts for comparison to obtain more detailed insights into changes in cellular function. Firstly, metabolic changes have been extensively studied in recent years. The 108 metabolic signaling pathways were selected for further analysis. The findings indicated that pathways such as selenoamino acid metabolism, propanoate metabolism, and ascorbate and aldarate metabolism were downregulated in Scissor+ SMCs, while pathways associated with keratan sulfate keratin metabolism, diseases of metabolism, arachidonic acid metabolism, and diseases associated with glycosaminoglycan metabolism were upregulated (Figure 3D). Secondly, the opening and closing of ion channels are crucial for regulating cellular functions and the internal environment. In Scissor+ SMCs, Ca2 activated K channels and ion channel transport pathways are significantly downregulated (Figure 3E). Finally, post-translational modification of proteins plays a crucial role in altering their function and activity. In Scissor+ SMCs, almost all post-translational modifications are diminished, with the most significant reduction observed in ubiquitination (Figure 3F). In summary, these findings underscore the significant alterations in cellular functions and regulatory mechanisms between Scissor+ SMCs and Scissor- SMCs.

Difference of Cellular Potency Category and Potency Score

According to the results from CytoTRACE 2 package, the proportions of "Unipotent" and "Oligopotent" cells in the cellular potency category for Scissor- SMCs were approximately 1.6% and 3.7% respectively. In contrast, these proportions were significantly reduced in Scissor+ SMCs, with both potency categories accounting for only 0.2% of all cells (Figure 4A–E). A comparison of the efficacy scores between Scissor+ and Scissor- SMCs, using the Wilcox rank-sum test, indicated a p value of less than 2.22e-16 (Figure 4F). This suggested that the potency score for Scissor+ SMCs is significantly lower than that for Scissor- SMCs, indicating that the majority of cells in the Scissor+ subgroup were in a differentiated state.

Differentially Expressed Genes

Differential expression analysis was performed on the gene expression matrix of Scissor+ SMCs and Scissor- SMCs, using the criteria of p_val_adj < 0.05 and $|\log_2 FC| > 1$. A total of 1063 DEGs were identified, including 677 upregulated genes. The limma package was utilized to perform differential expression analysis on 72 diseased samples and 32 normal

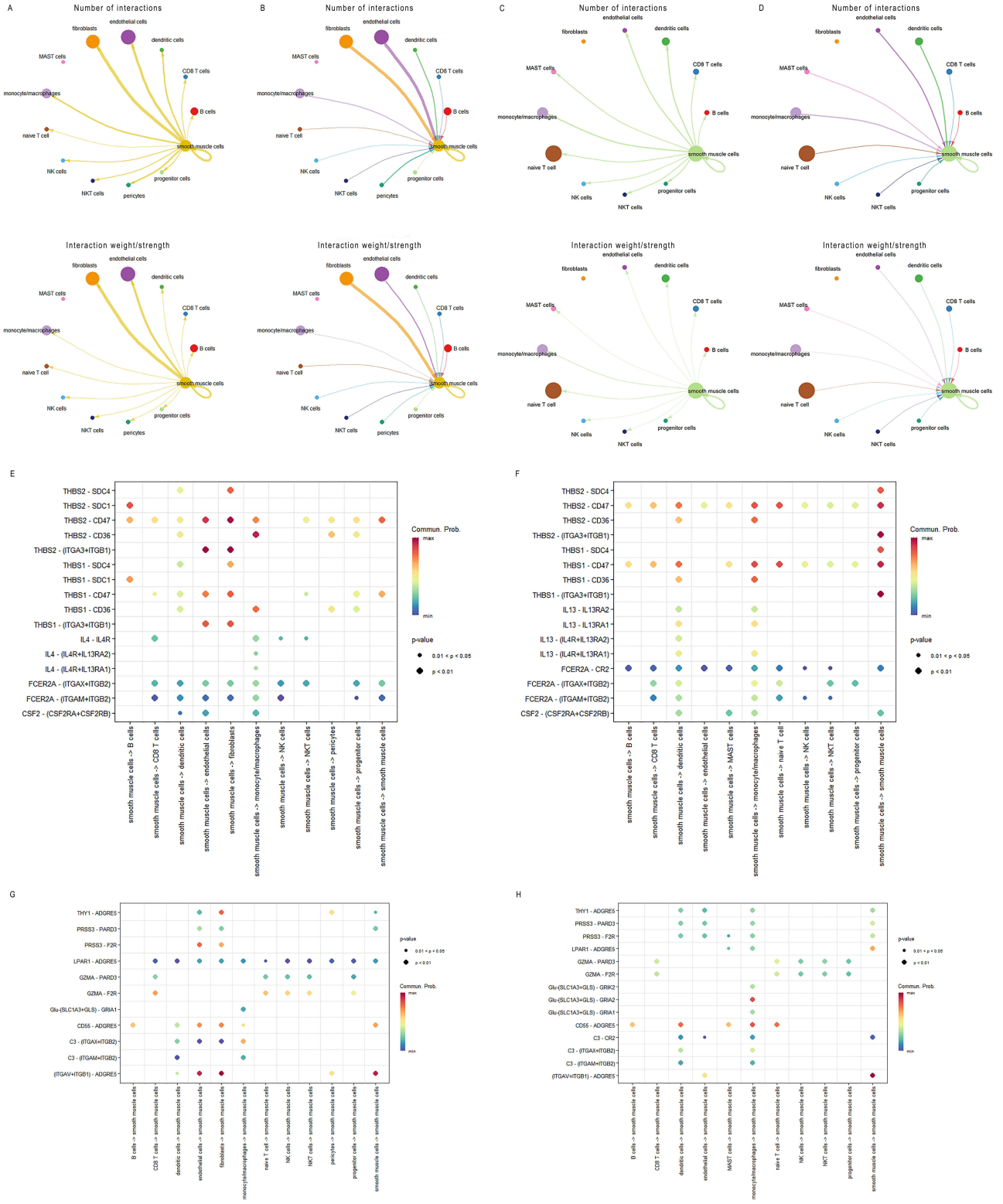

Figure 2 Cell-cell communication network. (**A**) Scissor+ SMCs as source in the cell communication network. (**B**) Scissor+ SMCs as target in the cell communication network. (**C**) Scissor- SMCs as source in the cell communication network. (**D**) Scissor- SMCs as target in the cell communication network. (**E** and **F**) The pathway with the most significant differences between Scissor+ cells and Scissor- cells when SMCs act as source. (**G** and **H**) The pathway with the most significant differences between Scissor+ cells and Scissor- cells when SMCs act as target.

https://doi.org/10.2147/JIR.S519114

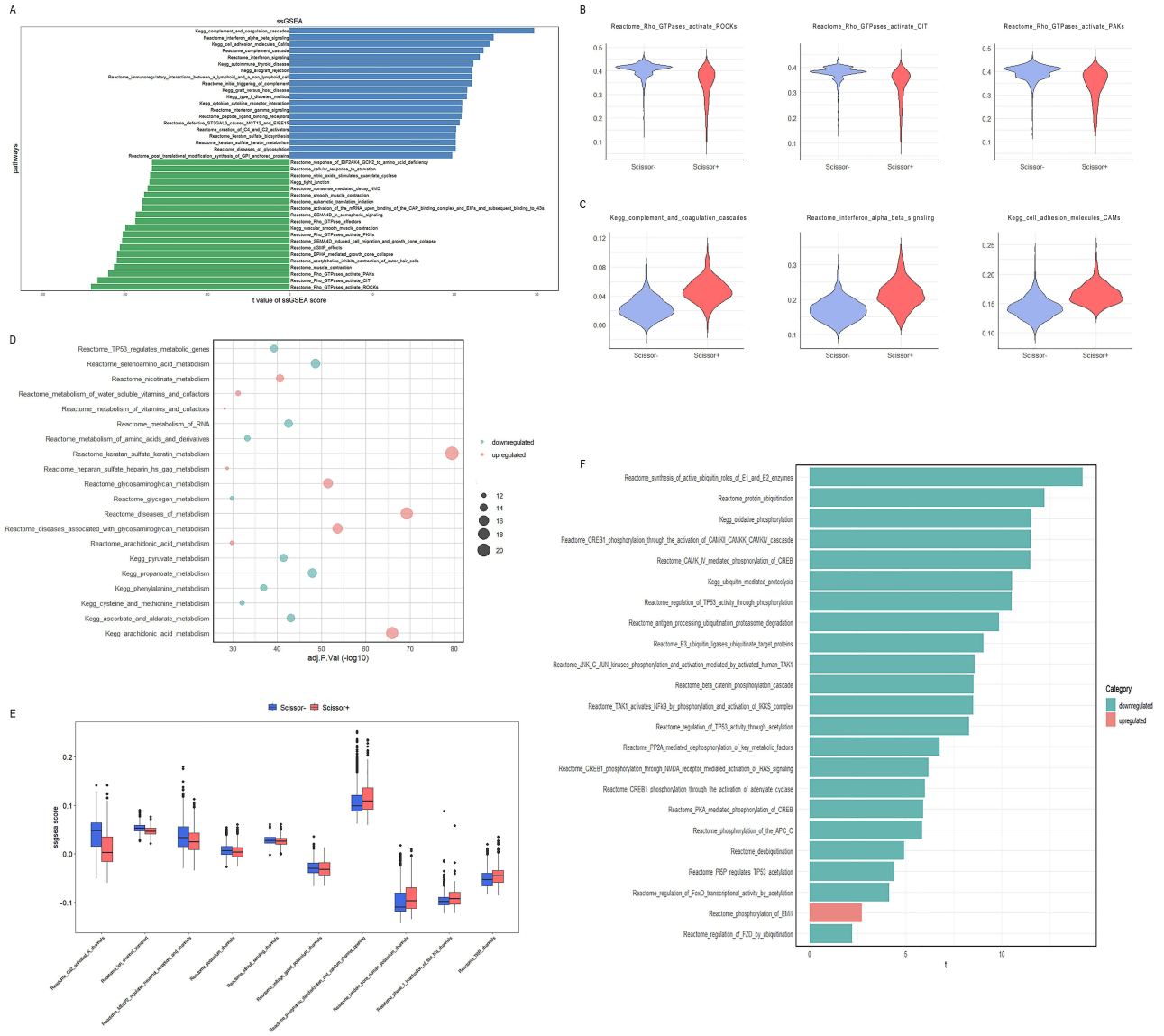

Figure 3 Cellular function enrichment. (**A**) The top 10 signaling pathways exhibiting the most significant upregulation and the top 10 signaling pathways demonstrating the most significant downregulation. (**B**) The violin plot of three most significantly downregulated pathways in Scissor+ SMC. (**C**) The violin plot of three most significantly upregulated pathways in Scissor+ SMC. (**D**) The bubble plot of the metabolic signaling pathway with the most significant differential expression. (**E**) The boxplot of channel pathways in Scissor+ SMCs and Scissor- SMCs. (**F**) The histogram of protein post-translational modification pathways.

samples. Then, DEGs were extracted which were simultaneously existed in both scRNA seq and array data. Subsequently, the intersection of the 50 most significantly upregulated DEGs in array data and the top 50 upregulated genes from scRNA-seq yielded a total of 20 differentially expressed genes (Figure 5A–D). These 20 genes were subsequently used for machine learning analysis. Subsequently, the clusterProfiler package was employed to perform GO enrichment analysis on all the upregulated DEGs. The results indicated that these DEGs are mainly associated with biological processes and molecular functions that promote inflammation, including antigen processing and presentation, positive regulation of cell adhesion, and MHC protein complex binding (Figure 5E–G). The main functions of these DEGs were related to promoting inflammation rather than normal functions such as SMCs contraction. This also suggests that Scissor+ SMCs may be transitioning from a contractile phenotype to a synthetic phenotype.

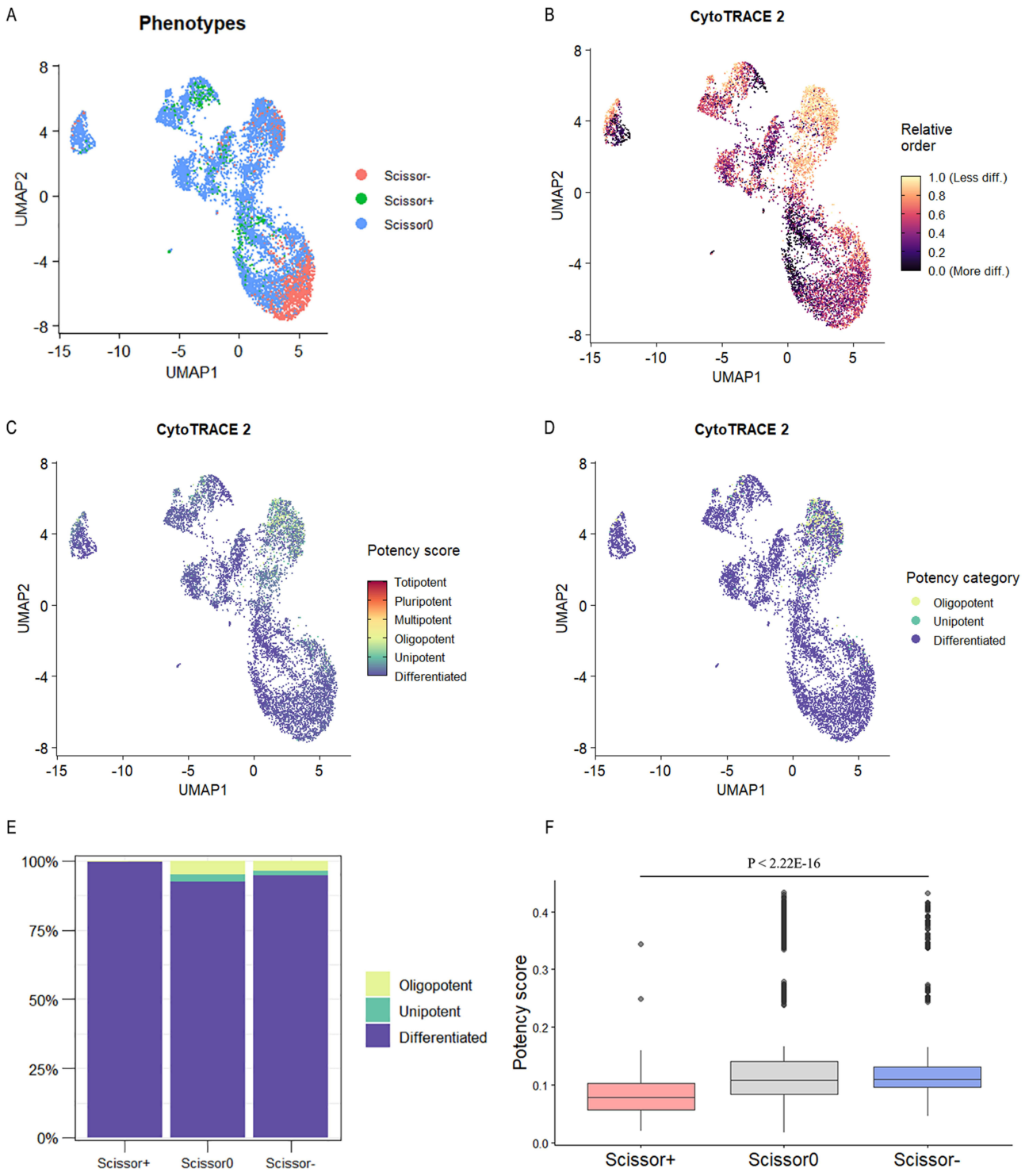

Figure 4 Cellular potency prediction. (**A**) The UMAP plot of the SMCs identified by Scissor package. (**B**) The UMAP plot of the relative order for SMCs. (**C**) The UMAP plot of potency score for SMCs. (**D**) The UMAP plot of potency category for SMCs. (**E**) The proportion of each potency category in three subgroups of SMCs. (**F**) The statistics of potency score for the three subgroups of SMCs and the statistical analysis between Scissor+ SMCs and Scissor- SMCs using Wilcox.

Machine Learning

In machine learning, independent variables such as DEGs are referred to as features. In the RF analysis, where ntree was set to 600 trees, the confusion matrix indicated an estimated error rate of 17.31% (Figure 6A and B). Leave-one-out cross-validation suggested that the error rate of the test results gradually increases as the number of features exceeds 10

https://doi.org/10.2147/JIR.S519114

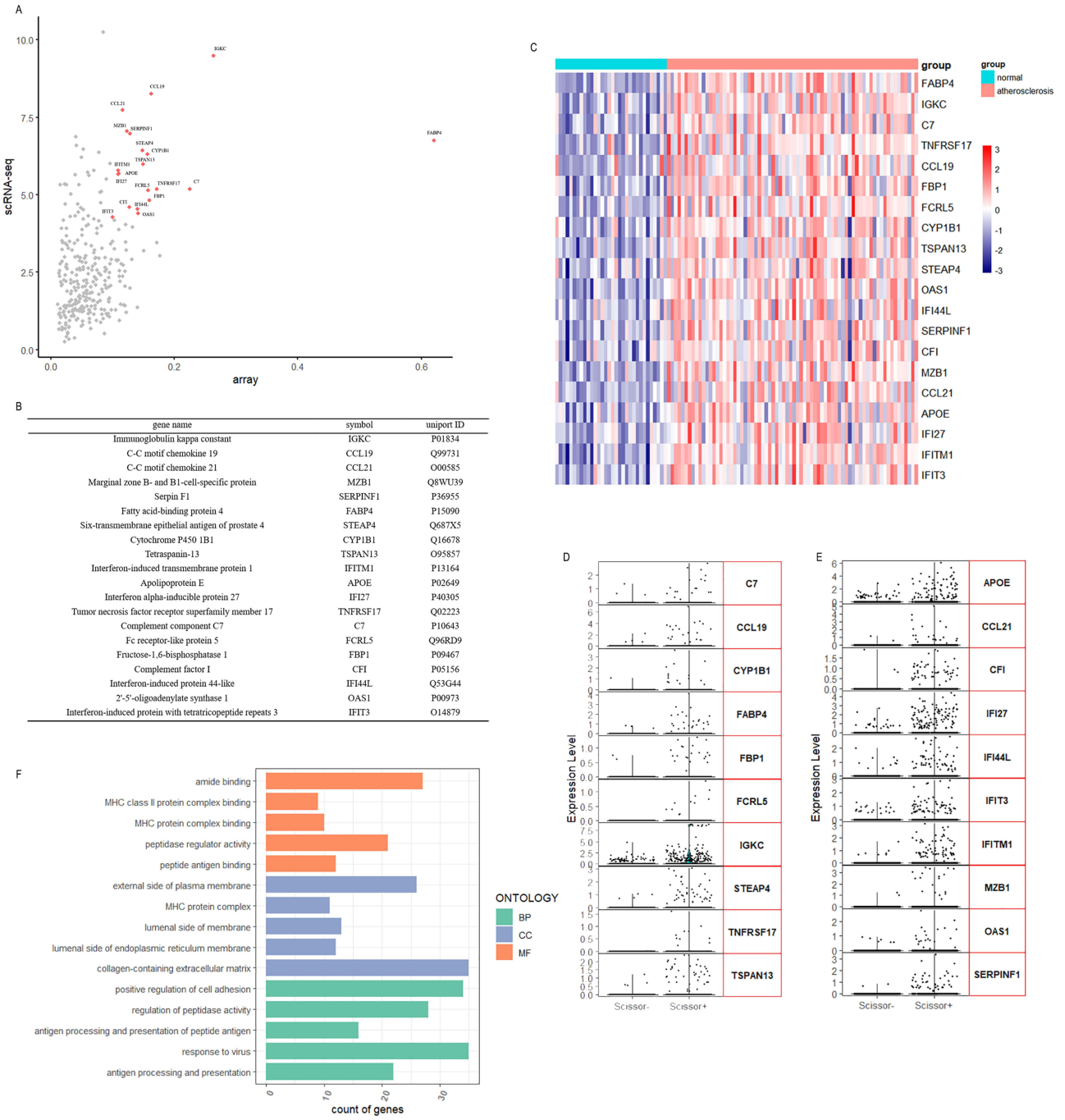

gene name	symbol	uniport ID
Immunoglobulin kappa constant	IGKC	P01834
C-C motif chemokine 19	CCL19	Q99731
C-C motif chemokine 21	CCL21	O00585
Marginal zone B- and B1-cell-specific protein	MZB1	Q8WU39
Serpin F1	SERPINF1	P36955
Fatty acid-binding protein 4	FABP4	P15090
Six-transmembrane epithelial antigen of prostate 4	STEAP4	Q687X5
Cytochrome P450 1B1	CYP1B1	Q16678
Tetraspanin-13	TSPAN13	O95857
Interferon-induced transmembrane protein 1	IFITM1	P13164
Apolipoprotein E	APOE	P02649
Interferon alpha-inducible protein 27	IFI27	P40305
Tumor necrosis factor receptor superfamily member 17	TNFRSF17	Q02223
Complement component C7	C7	P10643
Fc receptor-like protein 5	FCRL5	Q96RD9
Fructose-1,6-bisphosphatase 1	FBP1	P09467
Complement factor I	CFI	P05156
Interferon-induced protein 44-like	IFI44L	Q53G44
2'-5'-oligoadenylate synthase 1	OAS1	P00973
Interferon-induced protein with tetratricopeptide repeats 3	IFIT3	O14879

Figure 5 The differentially expressed genes in scRNA-seq and array data. (**A**) The Log_2FC of gene symbols in scRNA-seq and array data, and the 20 most upregulated symbols in both scRNA-seq and array were marked in red. (**B**) The information of the 20 most upregulated symbols. (**C**) The relative expression of the 20 DEGs in array data. (**D** and **E**) The expression of the 20 DEGs in Scissor+ SMCs and Scissor- SMCs. (**F**) The GO enrichment results of all upregulated DEGs, the top 5 entries with the smallest P values were selected from each category.

(Figure 6C). Therefore, the top 10 features were selected based on MeanDecreaseGini values, sorted as follows: TNFRSF17, FABP4, IFITM1, OAS1, MZB1, FCRL5, CCL19, TSPAN13, IFIT3, and CCL21 (Figure 6D). Regarding LASSO regression, cross-validation revealed that lambda.min was equal to 0.01266 and lambda.1se was equal to 0.05111 (Figure 6E). The LASSO regression showed that 8 features significantly associated with atherosclerosis: FABP4, TNFRSF17, STEAP4, MZB1, CCL21, IFI27, IFITM1, and IFIT3. In this process, lambda.min was applied for the analysis, with L1 norm facilitating feature selection and model simplification (Figure 6F). According to cross-validation,

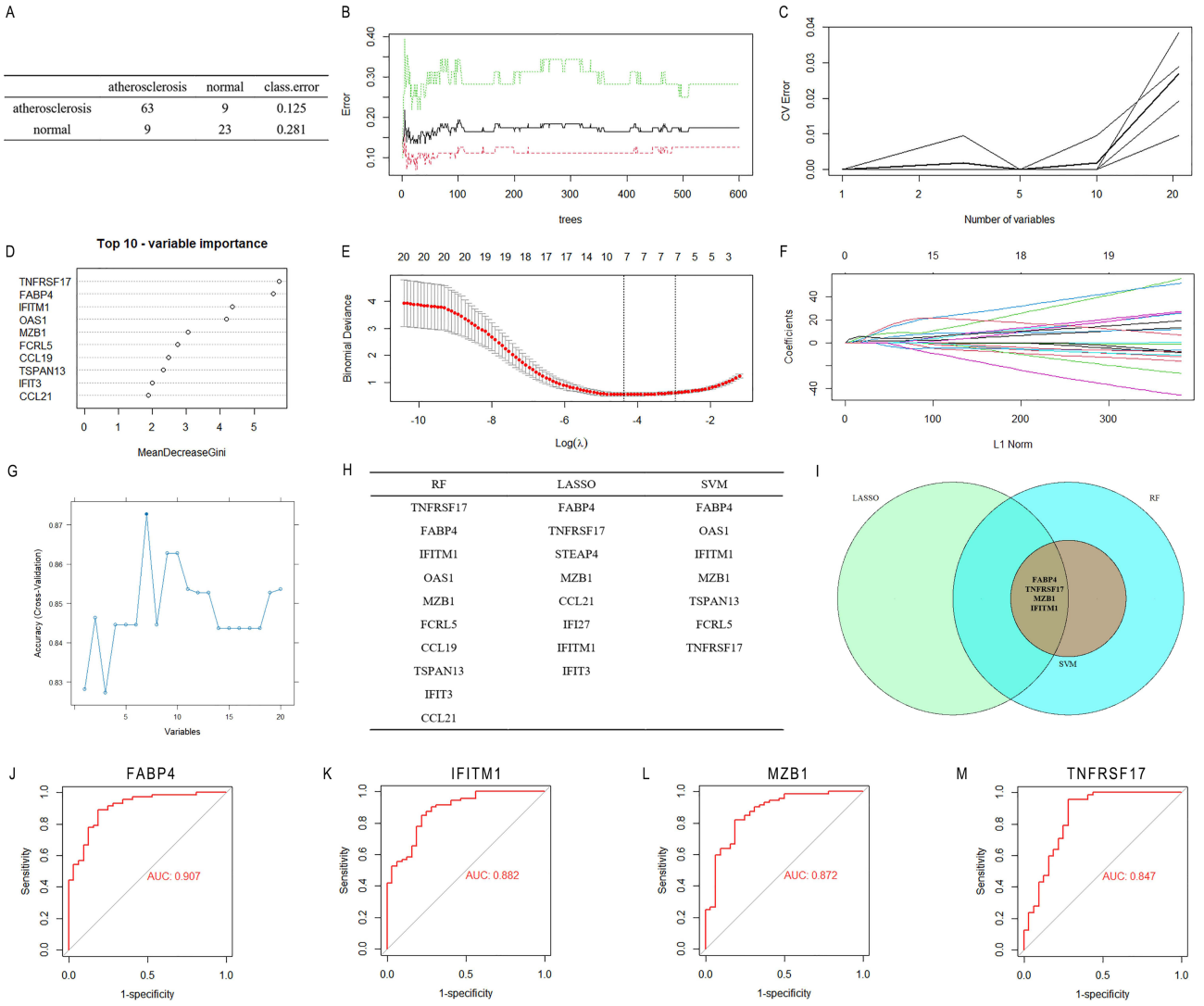

Figure 6 Machine learning. (**A**) The confusion matrix of RF. (**B**) The error rate plot of RF. In the plot, the red line represented the model error rate of the atherosclerosis group, the green line represented that of the healthy control group, and the black line represented the overall error rate. (**C**) The cross validation of RF (**D**) The top 10 features in RF ranking by MeanDecreaseGini values. (**E**) The cross validation of LASSO regression. (**F**) The plot of regularization path in LASSO regression. (**G**) The accuracy of model with the number of features changing in SVM. (**H**) The features associated atherosclerosis in the three models. (**I**) The intersection of the three models. (**J**) ROC curves of FABP4. (**K**) ROC curves of IFITM1. (**L**) ROC curves of MZB1. (**M**) ROC curves of TNFRSF17.

the SVM model demonstrates optimal accuracy with a feature value count of 7, which contained FABP4, OAS1, IFITM1, MZB1, TSPAN13, FCRL5, and TNFRSF17 (Figure 6G). The intersection of the 3 approaches yielded 4 features (Figure 6H and I). Through the pROC package, diagnostic models were constructed for these 6 features, ranked by their respective AUC values from highest to lowest: FABP4 (0.907), IFITM1 (0.882), MZB1 (0.872), TNFRSF17 (0.847) (Figure 6J–M). FABP4, with the highest AUC of 0.907, emerged as the feature most closely associated with atherosclerosis. This protein likely plays a critical role within specific subgroups of atherosclerosis-associated SMCs, highlighting its potential significance in disease pathology.

In vitro Experiments to Verify Differential Expression

Western blot was employed to detect the expression of ACTA2, an indicator of the contractile phenotype in MOVAS. The results showed that after MOVAS cells were stimulated with 25 μg/mL of ox-LDL for 4 days, the expression of ACTA2 was significantly decreased ($P < 0.0001$) (Figure 7A). This finding suggested that the MOVAS under this condition were allowed for subsequent qRT-PCR detection. Subsequently, the results of qRT-PCR showed that, after stimulating

https://doi.org/10.2147/JIR.S519114

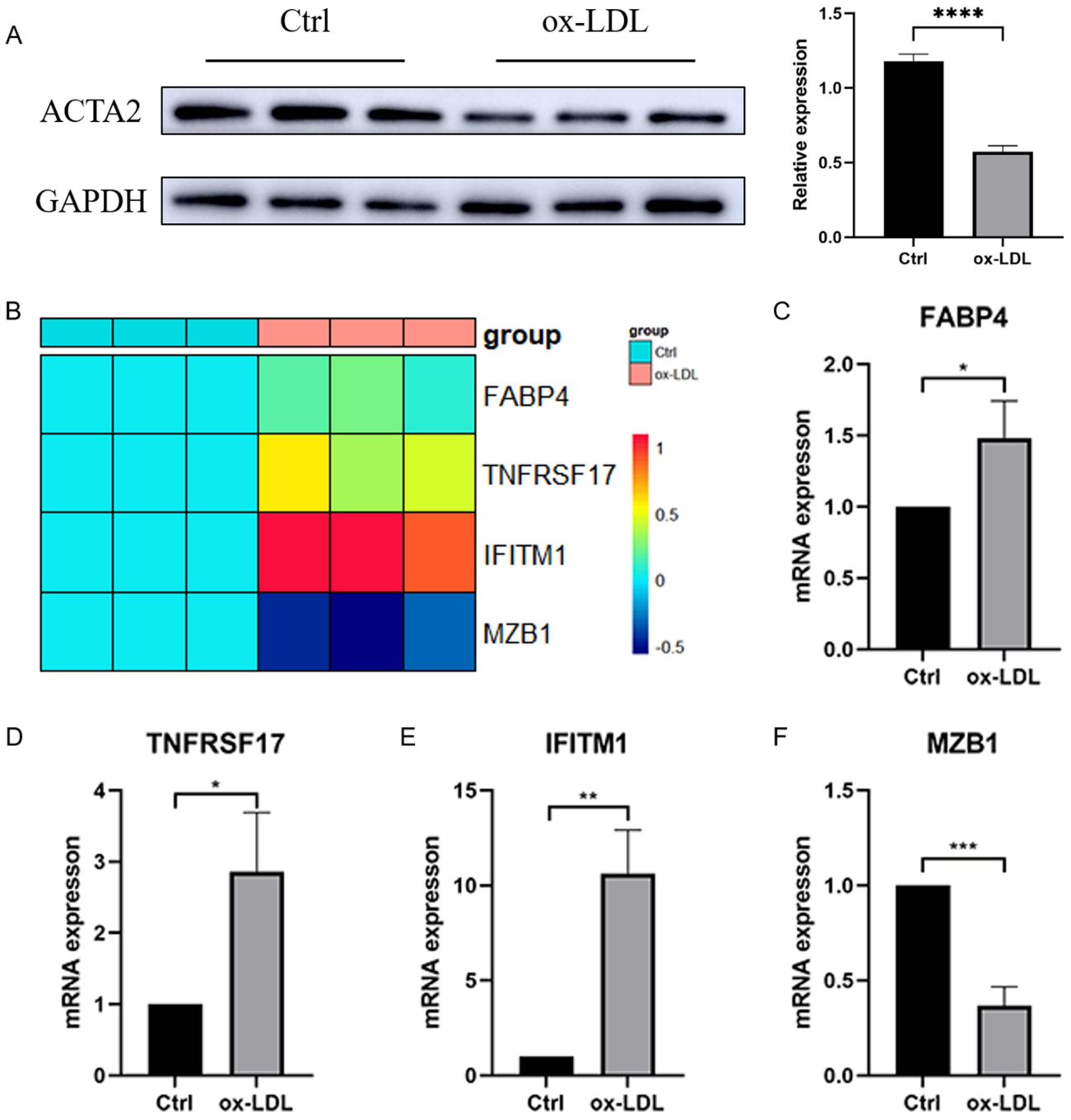

Figure 7 The validation result of DEGs. (**A**) The expression of ACTA2 was detected by Western blot. (**B**) The relative expression of the qRT-PCR result. (**C**–**F**) The statistical analysis of FABP4 (**B**), TNFRSF17 (**C**), IFITM1 (**D**) and MZB1 (**E**). *: *P* value < 0.05, **: *P* value < 0.01, ***: *P* value < 0.001, ****: *P* value < 0.0001.

MOVAS with of ox-LDL, the expression levels of FABP4 ($P < 0.05$), TNFRSF17 ($P < 0.05$), and IFITM1 ($P < 0.01$) were all upregulated compared to the control group. Notably, IFITM1 showed the most significant upregulation. Interestingly, the mRNA expression of MZB1 ($P < 0.001$) was opposite to the scRNA-seq data and array data, showing a decreasing trend (Figure 7B–F). Since the changes in the expression levels of FABP4, TNFRSF17, and IFITM1 in in vitro experiments were consistent with the sequencing results, in combination with the machine learning results, FABP4, which is most closely related to atherosclerosis among them, was selected for subsequent drug prediction and validation analysis.

Drug Prediction and Validation

The DGIdb database predicted a total of 27 compounds capable of binding to FABP4, all of which are inhibitors. Among these 27 inhibitors, 25 compounds have been confirmed to have binding sites with FABP4[44] (Figure S3), while two compounds, S-RP-6306 and PD166285, have not been verified. From the PubChem database, we obtained the SDF file for 3D structure of PD166285 and 2D structure of (S)-RP-6306 (only the SDF file of 2D structure was available for (S)-RP-6306). ChemBio3D software was used to calculate the lowest energy for these two compounds, with minimum energies of 60.7761 kcal/mol for (S)-RP-6306 and 63.7673 kcal/mol for PD166285. The crystal structure of FABP4 was obtained from the PDB database, in which the identity is 4NNS. We performed operations such as adding hydrogen to the protein and calculating the active grid of the protein, with the center of the grid located at x= −7.696, y= 9.575, z= −15.084. The results of molecular docking showed that (S)-RP-6306 had the lowest binding energy of −8.8 kcal/mol. Using PyMOL software to calculate the binding site at this binding energy, we found that (S)-RP-6306 forms a stable structure by forming a polar bond with the Arg-126 residue of FABP4, with a bond length of 2.6Å (Figure 8A and B). On the other hand, PD166285 had a minimum binding energy of −7.1 kcal/mol. PyMOL calculated that the binding site of this compound with FABP4 is the ASP-98 residue, and they are bound by a polar bond with a bond length of 2.2Å (Figure 8C and D). Among these two compounds, (S)-RP-6306 binds more stably to FABP4 and may be a potential therapeutic drug for further research on FABP4. Subsequently, MOVAS were stimulated with varying concentrations of (S)-RP-6306. The results indicated that the IC50 of this compound was 0.44 μM (Figure 8E). To prevent the death of MOVAS caused by simultaneous stimulation with (S)-RP-6306 and oxidized low-density lipoprotein (ox-LDL), MOVAS cells were co-stimulated with 0.2 μM of (S)-RP-6306 and ox-LDL. The qRT-PCR results revealed that (S)-RP-6306 could significantly reduce the expression level of FABP4 ($P < 0.0001$) (Figure 8F). Meanwhile, the expression level of ACTA2, a marker protein for the contractile phenotype of MOVAS, increased compared with that in the ox-LDL group and returned to the normal level ($P < 0.0001$) (Figure 8G). This finding validates the accuracy of the prediction, suggesting that (S)-RP-6306 can serve as an inhibitor of FABP4 for subsequent research.

Discussion

In this study, the Scissor package was utilized to integrate scRNA-seq data with array data, enabling the identification of a specific subgroup of SMCs strongly associated with the atherosclerotic phenotype. These cells exhibited high expression levels of FABP4. Cell-cell communication analysis revealed a significant enhancement in the interaction between SMCs and ECs among Scissor+ cells. Additionally, there was an increase in pro-inflammatory communication involving CD23, THBS, Complement, and PARs. Functionally, this subgroup demonstrated low expression of Rho-related pathways, whereas complement and coagulation cascades were notably upregulated. Meanwhile, CytoTRACE 2 package indicated that the potency score of Scissor+ SMCs was relatively lower than Scissor- SMCs, which indicated that Scissor+ SMCs have a tendency to transdifferentiate into other cells Through the application of machine learning, it was determined that the FABP4 protein demonstrates strong diagnostic efficacy for atherosclerosis. Furthermore, drug prediction and molecular docking analysis identified the compound (S)-RP-6306 as a stable binder to FABP4, exerting inhibitory effects, thus presenting a potential therapeutic option worthy of further investigation.

In the qRT-PCR results, the mRNA expression of FABP4, TNFRSF17, and IFITM1 were consistent with the scRNA-seq and array data. However, the expression of MZB1 shows an opposite trend. MZB1 has been reported to promote IgM and IgA secretion.[45] Studies have found that overexpression of MZB1 restored mitochondrial function and inhibited apoptosis in SMCs.[46] Therefore, in the sequencing data, MZB1 may be upregulated over the long term of atherosclerosis to counteract SMCs damage, while the expression level does not increase in the in vitro model due to the shorter time.

FABP4 is mainly overexpressed in macrophages and adipocytes. In macrophages, FABP4 inhibits the ATP-binding cassette A1 mediated by peroxisome proliferator-activated receptor gamma/ liver X receptor alpha, thereby promoting foam cell formation.[47] In FABP4-deficient macrophages, the expression of pro-inflammatory cytokines tumor necrosis factor alpha and monocyte chemoattractant protein-1 is reduced, potentially mediated by sirtuin 3.[48] In adipocytes, FABP4 undergoes acetylation, which exacerbates lipid storage and contributes to insulin resistance in subcutaneous adipose tissue, further worsening obesity.[47,49] With the application of scRNA-seq technology, a subgroup of ECs with high FABP4 expression has been identified in atherosclerotic tissues.[50] However, research on FABP4 in SMCs is still

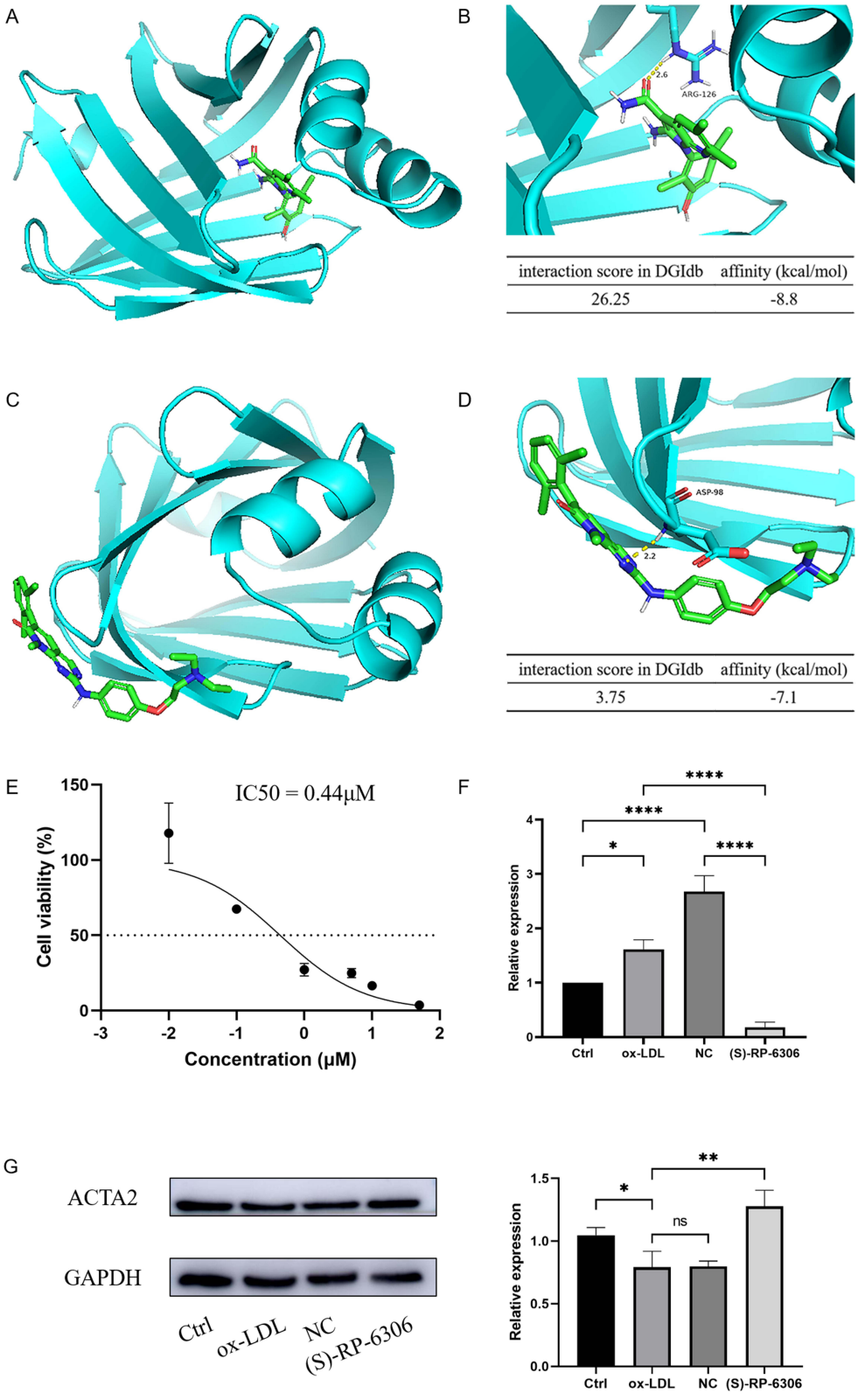

Figure 8 The drug prediction and validation. (**A** and **B**) The binding sites and binding energies of (S)-RP-6306 interacting with FABP4. (**C** and **D**) The binding sites and binding energies of PD166285 interacting with FABP4. (**E**). IC50 curve, with $\log_{10}$ (drug concentration) on the x-axis and cell viability on the y-axis. (**F**). The mRNA expression of FABP4 in MOVAS cells after stimulation with ox-LDL and (S)-RP-6306. (**G**) The protein expression of ACTA2 in MOVAS cells after stimulation with ox-LDL and (S)-RP-6306. *: *P* value < 0.05, **: *P* value < 0.01, ****: *P* value < 0.0001.

limited. Only one article reported that high FABP4 expression could mediate the MAPK signaling pathway to induce SMCs proliferation and migration, which contributes to atherosclerotic plaque formation.[51]

SMCs and their derived cells are involved in the pathogenesis of atherosclerosis. This study found that the expression of FABP4 in Scissor+ SMCs was approximately 90 times higher than in Scissor- SMCs. We ever doubted that these high FABP4-expressing SMCs might be transdifferentiated macrophages. However, comparing the expression levels of CD68 and ACTA2, we observed that CD68 expression was significantly lower than macrophage-annotated cells in this study, while ACTA2 expression was comparable to that in SMCs ($log_2FC<1$). Therefore, we proposed that these high FABP4-expressing SMCs represent a distinct subgroup of SMCs.

In addition, the subgroup of SMCs with high FABP4 expression exhibited strong inflammatory responses and inhibition of Rho-related pathways in our study. This suggests that the SMCs in this subgroup have lost their contractile function. The Rho-related pathways play a crucial regulatory role in contraction and other functions in SMCs. The Rho protein family, mainly including RhoA, RhoB, and RhoC, is involved in cellular activities such as cell migration, contraction, vesicle transport, and proliferation.[52] Among these, RhoA and Rho-associated protein kinase 1 (ROCK1) have been extensively studied in the context of SMCs. The activation of RhoA/ROCK1 enhances the sensitivity of SMCs to calcium-mediated contraction, with myosin light chain phosphorylation and myosin light chain kinase playing supportive roles.[53] Syndecan-4, a membrane protein, positively regulates the expression of RhoA and maintains the contractile phenotype of SMCs.[54] Recent studies have shown that the contractile phenotype of SMCs is regulated by the balance between RhoA and Rac1. RhoA alone maintains the contractile phenotype of SMCs; however, when the activity of Rac1 exceeds RhoA, it leads to the dedifferentiation of SMCs.[55]

Concurrently, the cellular communication between Scissor+ SMCs and Scissor+ ECs was significantly heightened. Prior research has disclosed that SMCs and ECs exchange various substances with one another through gap junctions, extracellular vesicles, and other mechanisms.[56,57] In our study, we also observed that communication between Scissor+ SMCs and Scissor+ ECs could be mediated through CD23, THBS, PARs, and complement. CD23 is considered to be expressed on the surface of B lymphocytes, and is a receptor with low affinity to immunoglobulin IgE.[58] It is mainly involved in allergic reaction, and its role in atherosclerosis is unknown. Among the other three pathways, THBS, also known as thrombospondin, is a type of protein that can associate with cell membrane and extracellular matrix. In atherosclerotic plaque, THBS enhanced localized inflammation and induced the migration of SMCs and ECs.[59] PARs, including PAR-1 and PAR-2, induced inflammatory responses in SMCs and ECs, similar to the effects of MAPK and NF-κB signaling pathways.[60] In vivo, the expression of VCAM-1 and ICAM-1 proteins in ECs decreased in mice with a knockout of the response gene to completion 32 protein, and the atherosclerotic plaques in the aorta of these mice were significantly reduced.[61] Although these studies have shown that the three proteins promoted migration and inflammatory responses in ECs and SMCs, the impact on intercellular communication between these two cell types has not yet been validated. Inhibiting these intercellular signaling pathways may offer a new approach for the treatment of atherosclerosis.

Machine learning indicated that FABP4 was highly effective in diagnosing atherosclerosis and shows a strong correlation with its pathogenesis. In drug prediction, (S)-RP-6306 demonstrated robust binding capabilities among inhibitors that have not yet been proven to interact with FABP4. RP-6306, initially developed as a highly bioavailable anti-tumor drug, inhibits the activity of membrane-associated tyrosine- and threonine-specific cdc2-inhibitory kinase and further suppresses the proliferation of tumor cells with high cyclin-E1 expression.[62,63] However, this study suggests that (S)-RP-6306, a stereoisomer of RP-6306, may have potential as a FABP4 inhibitor.

SMCs are integral components of the blood vessel wall and play a crucial role in the development and progression of atherosclerosis.[64] These cells are involved in various aspects of atherosclerotic disease, including plaque formation and vessel remodeling. In our study, we utilized a combination of multi-omics analysis and machine learning techniques to identify atherosclerosis-associated SMCs. This approach allowed us to screen for specific marker proteins that are indicative of the disease and to predict potential inhibitors that could be targeted for therapeutic intervention. By analyzing marker proteins, as well as differences in cell function, communication, and differentiation capabilities, we have gained valuable insights that could pave the way for new strategies in managing and potentially treating atherosclerosis. Despite these promising results, our study is limited by the lack of fundamental experimental validation. The

predictive marker FABP4 and the identified inhibitors need to be rigorously tested in laboratory settings to confirm their effectiveness and safety. Further experimental verification is essential to validate our findings and ensure that they can be translated into practical clinical applications. Continued research and validation efforts are necessary to fully establish the potential of these biomarkers and inhibitors in improving patient outcomes in atherosclerosis management and treatment.

Conclusion

In conclusion, our study revealed that atherosclerosis-associated SMCs (Scissor+ SMCs) exhibited high expression levels of FABP4. Analysis using LASSO regression, RF, SVM, and ROC curves all indicated a significant correlation between FABP4 and atherosclerosis. We observed notable differences in functional properties, cell-cell communication, and differentiation potential between Scissor+ SMCs and Scissor- SMCs. Additionally, compound (S)-RP-6306 was predicted to exhibit strong binding affinity with FABP4, suggesting its potential as an effective FABP4 inhibitor. This prediction has been further corroborated by in vitro experiments. Currently, SMCs play a particularly crucial role in the development of atherosclerosis. The above-mentioned results contribute to a deeper understanding of the cellular basis of atherosclerosis, providing a theoretical foundation for the development of treatment strategies targeting specific cell subsets and opening up new directions for drug research and development for atherosclerosis. However, this study is mainly based on bioinformatics analysis. Although in vitro experiments have been conducted for validation, in-vivo experimental data are still lacking. If (S)-RP-6306 can further demonstrate its efficacy and safety through in-vivo experiments and clinical trials, it is expected to become a novel drug for the treatment of atherosclerosis.

Abbreviations

scRNA-seq, single-cell RNA sequencing; RNA-seq, RNA sequencing; SMCs, smooth muscle cells; ECs, endothelial cells; MOVAS, murine aortic vascular smooth muscle cells; GEO, Gene Expression Omnibus; UMAP, uniform manifold approximation and projection; ssGSEA, single-sample gene set enrichment analysis; KEGG, Kyoto Encyclopedia of Genes and Genomes; DEGs, differentially expressed genes; LASSO, least absolute shrinkage and selection operator; RF, random forest; SVM, support vector machine; ROC, receiver operating characteristic; AUC, area under the curve; qRT-PCR, Quantitative reverse transcriptase polymerase chain reaction; DGIdb, Drug Gene Interaction Database; PDB, Protein Data Bank; FABP4, fatty acid-binding protein 4; IFITM1, interferon-induced transmembrane protein 1; MZB1, marginal zone B- and B1-cell-specific protein; TNFRSF17, tumor necrosis factor receptor superfamily member 17.

Data Sharing Statement

The scRNA-seq and array data (GSE155512, GSE159677, GSE43292 and GSE125771) were derived from GEO database (https://www.ncbi.nlm.nih.gov/geo/). The interaction between genes and compounds were obtained from DGIdb database (https://dgidb.org/). The structure of FABP4 was got from PDB database (https://www.rcsb.org/). The structure of (S)-RP-6306 and PD166285 were gained from PubChem database (https://pubchem.ncbi.nlm.nih.gov/).

Ethics Approval and Consent to Participate

Our study was a secondary analysis of publicly available data from multiple databases and no additional ethical approval was required.

Acknowledgments

We thank the Gene Expression Omnibus (GEO), Drug Gene Interaction Database (DGIdb), Protein Data Bank (PDB) and PubChem database for sharing a large amount of publicly available data. Moreover, we also thank the Jiangsu Commission of Health and Jiangsu Provincial Medical Youth Talent for their financial support in conducting this research. Finally, graphical abstract is created in BioRender. Wang, Y. (2025) https://BioRender.com/zpky0y4.

Author Contributions

All authors made a significant contribution to the work reported, whether that is in the conception, study design, execution, acquisition of data, analysis and interpretation, or in all these areas; took part in drafting, revising or critically reviewing the article; gave final approval of the version to be published; have agreed on the journal to which the article has been submitted; and agree to be accountable for all aspects of the work.

Funding

This research was generously supported by Jiangsu Commission of Health (No. H2018004) and Jiangsu Provincial Medical Youth Talent (No. QNRC2016837).

Disclosure

The authors declare that they have no competing interests in this work.

References

1. Libby P. The changing landscape of atherosclerosis. *Nature*. 2021;592(7855):524–533. doi:10.1038/s41586-021-03392-8
2. Libby P, Buring JE, Badimon L, et al. Atherosclerosis. *Nat Rev Dis Primers*. 2019;5(1):56. doi:10.1038/s41572-019-0106-z
3. Pattarabanjird T, Li C, McNamara C. B cells in atherosclerosis: mechanisms and potential clinical applications. *JACC Basic Transl Sci*. 2021;6(6):546–563. doi:10.1016/j.jacbts.2021.01.006
4. Hou P, Fang J, Liu Z, et al. Macrophage polarization and metabolism in atherosclerosis. *Cell Death Dis*. 2023;14(10):691. doi:10.1038/s41419-023-06206-z
5. Wang Y, Wang C, Li J. Neutrophil extracellular traps: a catalyst for atherosclerosis. *Mol Cell Biochem*. 2024;479(12):3213–3227. doi:10.1007/s11010-024-04931-3
6. Saigusa R, Winkels H, Ley K. T cell subsets and functions in atherosclerosis. *Nat Rev Cardiol*. 2020;17(7):387–401. doi:10.1038/s41569-020-0352-5
7. Soehnlein O, Libby P. Targeting inflammation in atherosclerosis - from experimental insights to the clinic. *Nat Rev Drug Discov*. 2021;20(8):589–610. doi:10.1038/s41573-021-00198-1
8. Zhai M, Gong S, Luan P, et al. Extracellular traps from activated vascular smooth muscle cells drive the progression of atherosclerosis. *Nat Commun*. 2022;13(1):7500. doi:10.1038/s41467-022-35330-1
9. Grootaert M, Bennett MR. Vascular smooth muscle cells in atherosclerosis: time for a re-assessment. *Cardiovasc Res*. 2021;117(11):2326–2339. doi:10.1093/cvr/cvab046
10. Zhang F, Guo X, Xia Y, Mao L. An update on the phenotypic switching of vascular smooth muscle cells in the pathogenesis of atherosclerosis. *Cell Mol Life Sci*. 2021;79(1):6. doi:10.1007/s00018-021-04079-z
11. Maiseyeu A, Di L, Ravodina A, et al. Plaque-targeted, proteolysis-resistant, activatable and MRI-visible nano-GLP-1 receptor agonist targets smooth muscle cell differentiation in atherosclerosis. *Theranostics*. 2022;12(6):2741–2757. doi:10.7150/thno.66456
12. Ma S, Motevalli SM, Chen J, et al. Precise theranostic nanomedicines for inhibiting vulnerable atherosclerotic plaque progression through regulation of vascular smooth muscle cell phenotype switching. *Theranostics*. 2018;8(13):3693–3706. doi:10.7150/thno.24364
13. Van de Sande B, Lee JS, Mutasa-Gottgens E, et al. Applications of single-cell RNA sequencing in drug discovery and development. *Nat Rev Drug Discov*. 2023;22(6):496–520. doi:10.1038/s41573-023-00688-4
14. Papalexi E, Satija R. Single-cell RNA sequencing to explore immune cell heterogeneity. *Nat Rev Immunol*. 2018;18(1):35–45. doi:10.1038/nri.2017.76
15. Jovic D, Liang X, Zeng H, Lin L, Xu F, Luo Y. Single-cell RNA sequencing technologies and applications: a brief overview. *Clin Transl Med*. 2022;12(3):e694. doi:10.1002/ctm2.694
16. Hao Y, Stuart T, Kowalski MH, et al. Dictionary learning for integrative, multimodal and scalable single-cell analysis. *Nat Biotechnol*. 2024;42(2):293–304. doi:10.1038/s41587-023-01767-y
17. Ritchie ME, Phipson B, Wu D, et al. limma powers differential expression analyses for RNA-sequencing and microarray studies. *Nucleic Acids Res*. 2015;43(7):e47. doi:10.1093/nar/gkv007
18. Leek JT, Johnson WE, Parker HS, Jaffe AE, Storey JD. The sva package for removing batch effects and other unwanted variation in high-throughput experiments. *Bioinformatics*. 2012;28(6):882–883. doi:10.1093/bioinformatics/bts034
19. Sun D, Guan X, Moran AE, et al. Identifying phenotype-associated subpopulations by integrating bulk and single-cell sequencing data. *Nat Biotechnol*. 2022;40(4):527–538. doi:10.1038/s41587-021-01091-3
20. Jin S, Plikus MV, Nie Q. CellChat for systematic analysis of cell-cell communication from single-cell and spatially resolved transcriptomics. *bioRxiv*. 2023. doi:10.1101/2023.11.05.565674
21. Hänzelmann S, Castelo R, Guinney J. GSVA: gene set variation analysis for microarray and RNA-seq data. *BMC Bioinf*. 2013;14(7). doi:10.1186/1471-2105-14-7
22. Kang M, Armenteros J, Gulati GS, et al. Mapping single-cell developmental potential in health and disease with interpretable deep learning. *bioRxiv*. 2024. doi:10.1101/2024.03.19.585637
23. Hu J, Szymczak S. A review on longitudinal data analysis with random forest. *Brief Bioinform*. 2023;24(2). doi:10.1093/bib/bbad002
24. Tay JK, Narasimhan B, Hastie T. Elastic net regularization paths for all generalized linear models. *J Stat Softw*. 2023;106(1). doi:10.18637/jss.v106.i01
25. Rodríguez-Pérez R, Bajorath J. Evolution of support vector machine and regression modeling in chemoinformatics and drug discovery. *J Comput Aided Mol Des*. 2022;36(5):355–362. doi:10.1007/s10822-022-00442-9

26. Robin X, Turck N, Hainard A, et al. pROC: an open-source package for R and S+ to analyze and compare ROC curves. *BMC Bioinf*. 2011;12(77). doi:10.1186/1471-2105-12-77
27. Cannon M, Stevenson J, Stahl K, et al. DGIdb 5.0: rebuilding the drug-gene interaction database for precision medicine and drug discovery platforms. *Nucleic Acids Res*. 2024;52(D1):D1227–D1235. doi:10.1093/nar/gkad1040
28. Kim S, Chen J, Cheng T, et al. PubChem 2023 update. *Nucleic Acids Res*. 2023;51(D1):D1373–D1380. doi:10.1093/nar/gkac956
29. Bittrich S, Segura J, Duarte JM, Burley SK, Rose Y. RCSB protein Data Bank: exploring protein 3D similarities via comprehensive structural alignments. *Bioinformatics*. 2024;40(6). doi:10.1093/bioinformatics/btae370
30. Depuydt M, Prange K, Slenders L, et al. Microanatomy of the human atherosclerotic plaque by single-cell transcriptomics. *Circ Res*. 2020;127 (11):1437–1455. doi:10.1161/CIRCRESAHA.120.316770
31. Voigt AP, Mulfaul K, Mullin NK, et al. Single-cell transcriptomics of the human retinal pigment epithelium and choroid in health and macular degeneration. *Proc Natl Acad Sci U S A*. 2019;116(48):24100–24107. doi:10.1073/pnas.1914143116
32. Bäckdahl J, Franzén L, Massier L, et al. Spatial mapping reveals human adipocyte subpopulations with distinct sensitivities to insulin. *Cell Metab*. 2021;33(9):1869–1882.e6. doi:10.1016/j.cmet.2021.07.018
33. Obradovic A, Chowdhury N, Haake SM, et al. Single-cell protein activity analysis identifies recurrence-associated renal tumor macrophages. *Cell*. 2021;184(11):2988–3005.e16. doi:10.1016/j.cell.2021.04.038
34. Schelker M, Feau S, Du J, et al. Estimation of immune cell content in tumour tissue using single-cell RNA-seq data. *Nat Commun*. 2017;8(1):2032. doi:10.1038/s41467-017-02289-3
35. Qi F, Zhang W, Huang J, Fu L, Zhao J. Single-Cell RNA sequencing analysis of the immunometabolic rewiring and immunopathogenesis of coronavirus disease 2019. *Front Immunol*. 2021;12:651656. doi:10.3389/fimmu.2021.651656
36. Anand P, Guillaumet-Adkins A, Dimitrova V, et al. Single-cell RNA-seq reveals developmental plasticity with coexisting oncogenic states and immune evasion programs in ETP-ALL. *Blood*. 2021;137(18):2463–2480. doi:10.1182/blood.2019004547
37. Zhu L, Cao Z, Wang S, et al. Single-cell transcriptomics reveals peripheral immune responses in anti-synthetase syndrome-associated interstitial lung disease. *Front Immunol*. 2022;13:804034. doi:10.3389/fimmu.2022.804034
38. Dinh HQ, Pan F, Wang G, et al. Integrated single-cell transcriptome analysis reveals heterogeneity of esophageal squamous cell carcinoma microenvironment. *Nat Commun*. 2021;12(1):7335. doi:10.1038/s41467-021-27599-5
39. Zhang L, Nie Q. scMC learns biological variation through the alignment of multiple single-cell genomics datasets. *Genome Biol*. 2021;22(1):10. doi:10.1186/s13059-020-02238-2
40. Valent P, Orazi A, Savona MR, et al. Proposed diagnostic criteria for classical chronic myelomonocytic leukemia (CMML), CMML variants and pre-CMML conditions. *Haematologica*. 2019;104(10):1935–1949. doi:10.3324/haematol.2019.222059
41. Brosseau JP, Sathe AA, Wang Y, et al. Human cutaneous neurofibroma matrisome revealed by single-cell RNA sequencing. *Acta Neuropathol Commun*. 2021;9(1):11. doi:10.1186/s40478-020-01103-4
42. Hoffmann D, Dvorakova T, Stroobant V, et al. Tryptophan 2,3-dioxygenase expression identified in human hepatocellular carcinoma cells and in intratumoral pericytes of most cancers. *Cancer Immunol Res*. 2020;8(1):19–31. doi:10.1158/2326-6066.CIR-19-0040
43. Gao S, Yan L, Wang R, et al. Tracing the temporal-spatial transcriptome landscapes of the human fetal digestive tract using single-cell RNA-sequencing. *Nat Cell Biol*. 2018;20(6):721–734. doi:10.1038/s41556-018-0105-4
44. Wang YT, Liu CH, Zhu HL. Fatty acid binding protein (FABP) inhibitors: a patent review (2012-2015). *Expert Opin Ther Pat*. 2016;26 (7):767–776. doi:10.1080/13543776.2016.1182500
45. Wei H, Wang J. Role of polymeric immunoglobulin receptor in IgA and IgM transcytosis. *Int J Mol Sci*. 2021;22(5):2284. doi:10.3390/ijms22052284
46. Zhu G, Li Y, Gao H, Li X, Fan H, Fan L. Mzb1 attenuates atherosclerotic plaque vulnerability in ApoE-/- mice by alleviating apoptosis and modulating mitochondrial function. *J Cardiovasc Transl Res*. 2024;17(4):782–794. doi:10.1007/s12265-024-10483-0
47. van der Ark-Vonk EM, Puijk MV, Pasterkamp G, van der Laan SW. The effects of FABP4 on cardiovascular disease in the aging population. *Curr Atheroscler Rep*. 2024;26(5):163–175. doi:10.1007/s11883-024-01196-5
48. Xu H, Hertzel AV, Steen KA, Bernlohr DA. Loss of fatty acid binding protein 4/aP2 reduces macrophage inflammation through activation of SIRT3. *Mol Endocrinol*. 2016;30(3):325–334. doi:10.1210/me.2015-1301
49. Navarro-Ruiz M, López-Alcalá J, Díaz-Ruiz A, et al. Understanding the adipose tissue acetylome in obesity and insulin resistance. *Transl Res*. 2022;246:15–32. doi:10.1016/j.trsl.2022.02.008
50. Lother A, Bergemann S, Deng L, Moser M, Bode C, Hein L. Cardiac endothelial cell transcriptome. *Arterioscler Thromb Vasc Biol*. 2018;38 (3):566–574. doi:10.1161/ATVBAHA.117.310549
51. Girona J, Rosales R, Plana N, Saavedra P, Masana L, Vallvé JC. FABP4 induces vascular smooth muscle cell proliferation and migration through a MAPK-dependent pathway. *PLOS ONE*. 2013;8(11):e81914. doi:10.1371/journal.pone.0081914
52. Eckenstaler R, Hauke M, Benndorf RA. A current overview of RhoA, RhoB, and RhoC functions in vascular biology and pathology. *Biochem Pharmacol*. 2022;206:115321. doi:10.1016/j.bcp.2022.115321
53. Sawma T, Shaito A, Najm N, et al. Role of RhoA and Rho-associated kinase in phenotypic switching of vascular smooth muscle cells: implications for vascular function. *Atherosclerosis*. 2022;358:12–28. doi:10.1016/j.atherosclerosis.2022.08.012
54. Hu J, Li Y, Wei Z, et al. A reduction in the vascular smooth muscle cell focal adhesion component syndecan-4 is associated with abdominal aortic aneurysm formation. *Clin Transl Med*. 2021;11(12):e605. doi:10.1002/ctm2.605
55. Talwar S, Kant A, Xu T, Shenoy VB, Assoian RK. Mechanosensitive smooth muscle cell phenotypic plasticity emerging from a null state and the balance between Rac and Rho. *Cell Rep*. 2021;35(3):109019. doi:10.1016/j.celrep.2021.109019
56. Johnson RD, Camelliti P. Role of non-myocyte gap junctions and connexin hemichannels in cardiovascular health and disease: novel therapeutic targets? *Int J Mol Sci*. 2018;19(3):866. doi:10.3390/ijms19030866
57. Raju S, Botts SR, Blaser MC, et al. Directional endothelial communication by polarized extracellular vesicle release. *Circ Res*. 2024;134 (3):269–289. doi:10.1161/CIRCRESAHA.123.322993
58. Engeroff P, Vogel M. The role of CD23 in the regulation of allergic responses. *Allergy*. 2021;76(7):1981–1989. doi:10.1111/all.14724
59. Forbes T, Pauza AG, Adams JC. In the balance: how do thrombospondins contribute to the cellular pathophysiology of cardiovascular disease? *Am J Physiol Cell Physiol*. 2021;321(5):C826–C845. doi:10.1152/ajpcell.00251.2021

60. Li Q, Yang XT, Wei W, Hu XP, Li XX, Xu M. Favorable effect of rivaroxaban against vascular dysfunction in diabetic mice by inhibiting NLRP3 inflammasome activation. *J Cell Physiol*. 2022;237(8):3369–3380. doi:10.1002/jcp.30807
61. Cui XB, Luan JN, Dong K, et al. RGC-32 (Response Gene to Complement 32) deficiency protects endothelial cells from inflammation and attenuates atherosclerosis. *Arterioscler Thromb Vasc Biol*. 2018;38(4):e36–e47. doi:10.1161/ATVBAHA.117.310656
62. Gallo D, Young J, Fourtounis J, et al. CCNE1 amplification is synthetic lethal with PKMYT1 kinase inhibition. *Nature*. 2022;604(7907):749–756. doi:10.1038/s41586-022-04638-9
63. Szychowski J, Papp R, Dietrich E, et al. Discovery of an orally bioavailable and selective PKMYT1 inhibitor, RP-6306. *J Med Chem*. 2022;65(15):10251–10284. doi:10.1021/acs.jmedchem.2c00552
64. Basatemur GL, Jørgensen HF, Clarke M, Bennett MR, Mallat Z. Vascular smooth muscle cells in atherosclerosis. *Nat Rev Cardiol*. 2019;16(12):727–744. doi:10.1038/s41569-019-0227-9